12th International Symposium on Turbulence and Shear Flow Phenomena (TSFP12)
Osaka, Japan, July 19–22, 2022

WALL-PRESSURE–VELOCITY TRANSFER KERNEL IN HIGH REYNOLDS NUMBER TURBULENT CHANNEL FLOWS

Woutijn J. Baars
Faculty of Aerospace Engineering
Delft University of Technology
2629 HS Delft, The Netherlands
w.j.baars@tudelft.nl

Myoungkyu Lee
Department of Aerospace Engineering and Mechanics
The University of Alabama
Tuscaloosa, AL 35487, U.S.A.
mklee@ua.edu

ABSTRACT

Since wall-pressure fluctuations would form a practically-robust input to a real-time active controller of wall-bounded turbulence, it is of high practical interest to study the scaling behavior of the wall-pressure–velocity coupling. This work investigates the coupling of the wall-pressure fluctuations with the streamwise and wall-normal velocity fluctuations. Both the gain (or coherence) and phase spectra of the wall-pressure–velocity transfer kernel are assessed using a comprehensive database, available from direct numerical simulations of turbulent channel flow. With data spanning a decade in friction Reynolds number $Re_\tau \sim 550-5200$, a 1D analysis (in terms of the streamwise wavelength, λ_x) reveals that the streamwise velocity and wall-pressure are most strongly coupled at a self-similar wall-scaling of $\lambda_x/y \approx 14$. For the wall-normal velocity component, the strongest coupling appears at approximately half this ratio ($\lambda_x/y \approx 8.5$). An analysis of the kernel's phase demonstrates that both the coherent fluctuations of streamwise and wall-normal velocity obey a forward-leaning inclination angle of $\alpha \approx 30^\circ$. When extending the analysis to 2D (as a function of λ_x and λ_z), the peak-coherence for p_w and u still resides close to $\lambda_x/y \approx 14$ and is reasonably symmetric around $\lambda_x/\lambda_z = 2.3$. The 2D coherence for p_w and v peaks around $\lambda_x/\lambda_z = 1.0$. Both the 2D coherence for p_w and u, and p_w and v, adhere to a wall-scaling with y. Scaling behaviours identified in this work will aid the efficacy of real-time controllers, by for instance the implementation of data-derived FIR filters to only control velocity structures that are captured through wall-pressure measurements.

INTRODUCTION AND CONTEXT

Inspiration for this work was born out of practical considerations associated with the implementation of real-time flow control of wall-bounded turbulence. Real-time opposition control is only effective when there is a significant degree of correlation between the grazing velocity fluctuations (consider those as the control 'targets') and a set of input sensors measuring the dynamic state of the boundary layer (Rathnasingham & Breuer, 2003; Brunton & Noack, 2015). For the case of wall-bounded turbulence, these sensors should be integrated within the wall itself to avoid form drag and, in this regard, a wall-pressure measurement is practically-robust and thus ideal in practise. Analyzing the statistical coupling between the velocity fluctuations in the boundary layer and the wall-pressure field is a pre-requisite to implementing a control system with a high 'observability' (Abbassi *et al.*, 2017; Samie *et al.*, 2020). Our work scrutinizes the statistical coupling, in the context of a linear time invariant system analysis. The notation in this paper is as follows. Coordinates x, y and z denote the streamwise, wall-normal and spanwise directions of the flow, and lower-case u, v, w and p represent the Reynolds decomposed fluctuations of the three velocity components and the static pressure, respectively. The wall-pressure is denoted as p_w. The friction Reynolds number $Re_\tau \equiv \delta u_\tau/\nu$ or δ^+ is the ratio of the channel half-width δ to the viscous length scale ν/u_τ.

Many works are concerned with scaling laws and modeling attempts of pressure fluctuations in wall-bounded turbulence (*e.g.,* Willmarth, 1975; Farabee & Casarella, 1991; Klewicki *et al.*, 2008; Hwang *et al.*, 2009), but a direct assessment of the instantaneous or statistical coupling between the fluctuating velocity field and the wall-pressure is required for wall-based velocity field estimations. Though, simultaneous measurements of turbulent velocities and p_w have already revealed characteristic wall-pressure signatures associated with burst-sweep cycle events (Thomas & Bull, 1983). Throughout the last decade, high-resolution mappings of the spatio-temporal pressure-velocity correlation have also been reported (Ghaemi & Scarano, 2013; Naka *et al.*, 2015), and have been extended to the spectral domain with the aid of coherence and phase spectra (most notably in the experimental works of Van Blitterswyk & Rocha, 2017; Gibeau & Ghaemi, 2021). Ex-

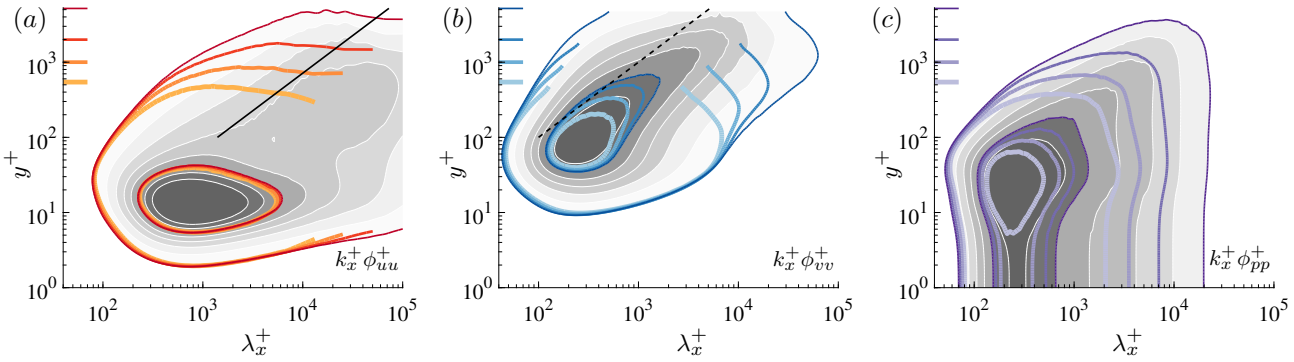

Figure 1: 1D spectrograms of (a) u, (b) v and (c) p. Two clusters of solid, coloured iso-contours on (a-c) correspond to two contour values of $k^+\phi_{uu}^+ = [0.2;\ 1.2]$, $k^+\phi_{vv}^+ = [0.05;\ 0.3]$ and $k^+\phi_{pp}^+ = [0.45;\ 2.25]$, respectively, for all Re_τ cases (an increased colour intensity corresponds to an increase in Re_τ; the channel half-widths $\delta^+ = Re_\tau$ are indicated along the ordinate). The gray-scale contour shows a finer discretization of iso-contours for the highest Reynolds number case only ($Re_\tau \approx 5200$).

perimental studies are subject to the inherent challenges associated with wall-pressure measurements, and performing those over a range of Re_τ in the absence of spatial/temporal resolution effects. In addition, it is challenging to simultaneously acquire velocity data (in a streamwise–spanwise plane) and the wall-pressure field. These data are required to investigate the wall-pressure–velocity coupling as a function of the energetic scales decomposed in their streamwise and spanwise Fourier modes. Novel experiments can be designed to yield 2D coherence spectra (*e.g.*, for velocity–velocity correlations, Deshpande *et al.*, 2020), but these are not trivial to conduct at a range of Re_τ without resolution effects entering the problem. We here analyse the wall-pressure–velocity kernel using the vast amount of high-fidelity data that is currently available from direct numerical simulation (DNS) campaigns.

Bode plots of the scale-dependent gain (or coherence) and phase for p_w and u, and p_w and v, are particularly useful for wall-based control. That is, a routine action for control would, for instance, involve an estimate of the streamwise velocity component u, at a wall-normal location y_e, based on p_w. When we for now confine ourselves to the x dimension only, a linear stochastic estimate $\widetilde{u}(x, y_e)$ can be generated, either with a time (Naguib *et al.*, 2001; Lasagna *et al.*, 2013) or spectral (Tinney *et al.*, 2006; Baars *et al.*, 2016) approach. An estimate in the spectral domain is denoted as $\widetilde{U}(\lambda_x, y_e) = H_L(\lambda_x, y_e)P_w(\lambda_x)$, where H_L is a complex-valued kernel and $\widetilde{U}(\lambda_x, y_e)$ and $P_w(\lambda_x)$ are the Fourier transforms of $\widetilde{u}(x, y_e)$ and $p_w(x)$, respectively. Note that $\lambda_x = 2\pi/k_x$ denotes the streamwise wavelength. The kernel is found from two-point calibration data and equals the complex-valued cross-spectrum, divided by the wall-pressure spectrum:

$$H_L(\lambda_x) = \frac{\phi_{up_w}(\lambda_x)}{\phi_{p_w p_w}(\lambda_x)} = |H_L(\lambda_x)| \cdot \exp^{j\psi(\lambda_x)}, \quad (1)$$

where the kernel's phase $\psi(\lambda_x)$ equals the phase of the cross-spectrum. The gain is often expressed in terms of a normalized, linear coherence with bounds of 0 and 1,

$$\gamma^2_{up_w}(\lambda_x) = |H_L(\lambda_x)|^2 \cdot \frac{\phi_{p_w p_w}(\lambda_x)}{\phi_{uu}(\lambda_x)}. \quad (2)$$

Note that the argument y_e is omitted in eqs. (1) and (2) for brevity. Even though the u velocity component was used above, the same can be done for v and w. And, as shown later, the analysis can be extended to 2D (*e.g.*, Encinar & Jiménez, 2019). Now this work investigates the scaling behavior of the kernel H_L, for p_w and the u and v velocities, with the aid of DNS data of turbulent channel flow.

DIRECT NUMERICAL SIMULATION DATA

Four channel flow datasets are used and span one decade in Reynolds number, $Re_\tau \sim 550 - 5200$ (see table 1 for exact values). Details on the numerical scheme, resolution and turbulence statistics can be found in Lee & Moser (2015, 2019). In relevance to the current work involving pressure, the static pressure fluctuations were obtained by solving a Poisson equation (Panton *et al.*, 2017). For reference, 1D spectrograms of u, v and p are shown in figs. 1a-c, respectively. Gray scale iso-contours correspond to the $Re_\tau \approx 5200$ dataset only, while the trends of how the spectrograms change with Re_τ are shown with two sets of coloured iso-contours, drawn for all Re_τ (see figure caption). The pressure spectrum remains constant for $y^+ \lesssim 5$, reflecting the wall-pressure spectrum. For all fluctuating quantities in fig. 1 it is evident that the total energy at a given y^+ grows due to the additional energetic scales at large λ_x^+. For instance, see Mathis *et al.* (2009) for the scaling of u-spectrograms and Panton *et al.* (2017) for the scaling of the mean-square pressure fluctuations.

Table 1: Channel DNS data (Lee & Moser, 2015).

Case name	R0550	R1000	R2000	R5200
Re_τ	544	1000	1995	5186

WALL-PRESSURE–VELOCITY COUPLING

Given the energy growth of the spectrograms in fig. 1, with an increase in Re_τ, it is of high interest to assess the Re_τ-trend in both the up_w and vp_w coherence.

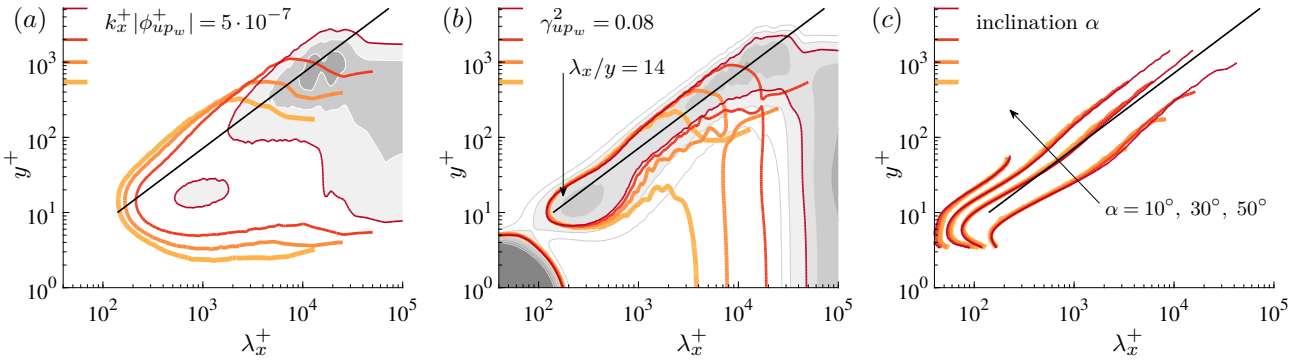

Figure 2: (a) 1D gain of the cross-spectrogram, computed using u and wall-pressure p_w. Solid, coloured iso-contours correspond to one contour value indicated in the figure, for all Re_τ cases (an increased colour intensity corresponds to an increase in Re_τ); the gray scale contour shows a finer discretization of iso-contours for $Re_\tau \approx 5200$ only. (b,c) Similar to sub-figure (a), but now for (b) the linear coherence of u and p_w and (c) the forward-leaning geometric phase angle α, as shown in fig. 4.

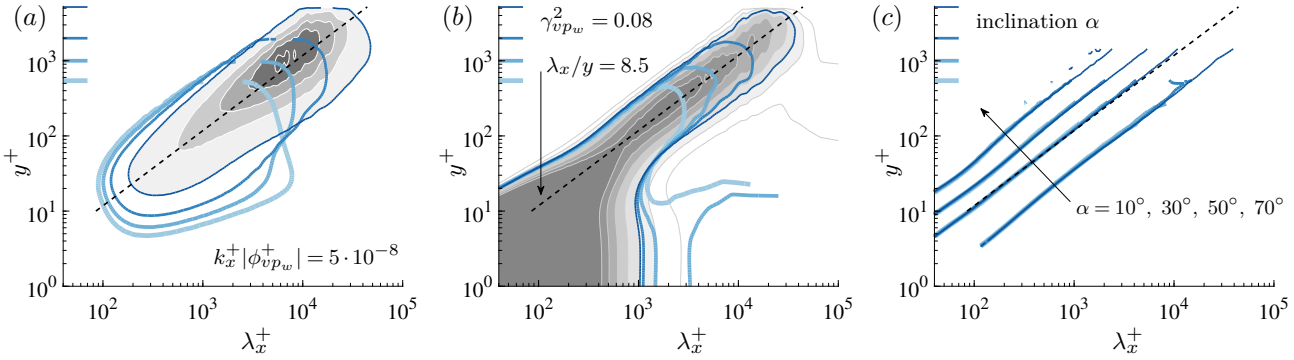

Figure 3: Similar to fig. 2 but for v and p_w, instead of u and p_w.

First we assess the coherence in the 1D, streamwise direction, since this is reminiscent of the confined view available from typical experiments.

1D analysis in the streamwise direction

Following eq. (1), the magnitude of the complex-valued cross-spectrum yields a first indication of the wall-pressure–velocity coupling. From the iso-contours of $|\phi^+_{up_w}|$ in fig. 2a it is evident that the degree of coupling grows self-similarly with an increase in Re_τ: the ridge in cross-spectral energy grows along the black solid line, which is representative of a wall scaling (constant $\lambda_x/y = 14$). This scaling is even more distinct when considering the coherence $\gamma^2_{up_w}$ in fig. 2b. Clearly, p_w and u are most strongly coupled at the self-similar scaling of $\lambda_x/y \approx 14$. This particular wall-scaling matches the Reynolds number invariant aspect ratio of wall-attached coherent structures of u, see Baars *et al.* (2017). The ridge of coherence is relatively narrow-band and only grows to larger viscous-scaled heights with increasing Reynolds number, not in width. It is surprising to note the appearance of a region of zero-coherence at relatively large wavelengths, and at locations below the ridge (which are in fact closer to the wall-pressure signature). This suggests that large-scale u fluctuations in close proximity to the wall do not comprise a phase-consistent relationship with the wall-pressure. Possibly due to the stronger dispersive (and random) nature in the convection of large-scale structures near the wall (Liu & Gayme, 2020). There is a region of non-zero coherence obeying an outer-scaling behavior at very large λ_x. This indicates that only the very large *global modes* in the velocity fluctuations, spanning the entire logarithmic region (del Álamo & Jiménez, 2003), leave a coherent wall-pressure footprint.

When focusing on the kernel's phase $\psi(\lambda_x)$ we convert the phase angle into a geometric inclination angle for ease of interpretation, following $\alpha(\lambda_x) \equiv \tan^{-1}(y/\Delta x)$, where $\Delta x = \lambda_x\psi(\lambda_x)/(2\pi)$ is the geometric phase shift. This procedure yields a geometric angle for each wavelength λ_x^+, and for each wall-normal location y^+, at which the turbulent velocity is assessed in relation to p_w. Fig. 2c shows iso-contours of constant $\alpha(\lambda_x)$, for all Re_τ cases. Fluctuations of u that are most wall-pressure-coherent (residing along $\lambda_x/y = 14$) lean forward with $\alpha \approx 30°$. Moreover, structures with higher and lower aspect ratios are less and more inclined, respectively. Finally, a perfect collapse of the different Re_τ curves indicates Reynolds number invariant behavior; this is of high practical importance when extrapolating wall-pressure–velocity filters to higher Re_τ flow control experiments.

Similar to the correlation analysis of p_w and u, the analysis can be performed with considering the v fluctuations instead. Findings are presented in fig. 3 and highlight that the wall-pressure-coherent energy in v resides at a smaller aspect ratio, around $\lambda_x/y \approx 8.5$ (note that the ridge of maximum coherence does not necessarily correspond to the ridge of maximum energy, as is

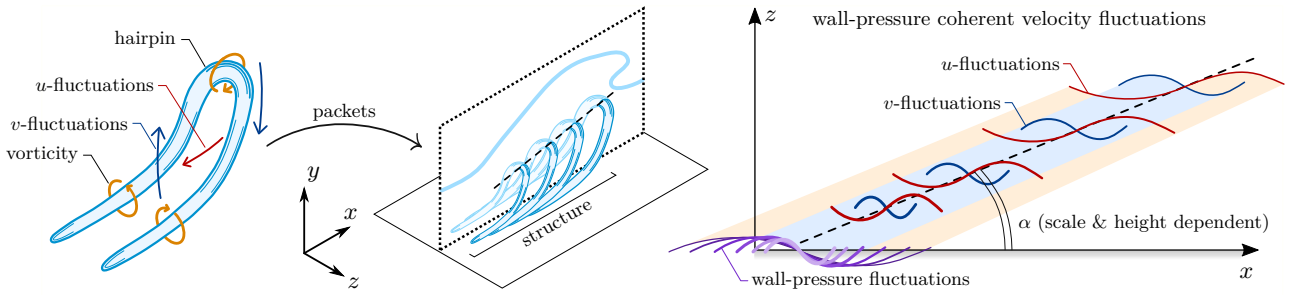

Figure 4: Illustration of hairpin packets and the statistical correlation between the wall-pressure, p_w, and the u- and v-velocity. Since the correlation and forward-leaning geometric phase angle α are dependent on scale and height, the coherent fluctuations are visualized as harmonic waves of varying streamwise scale.

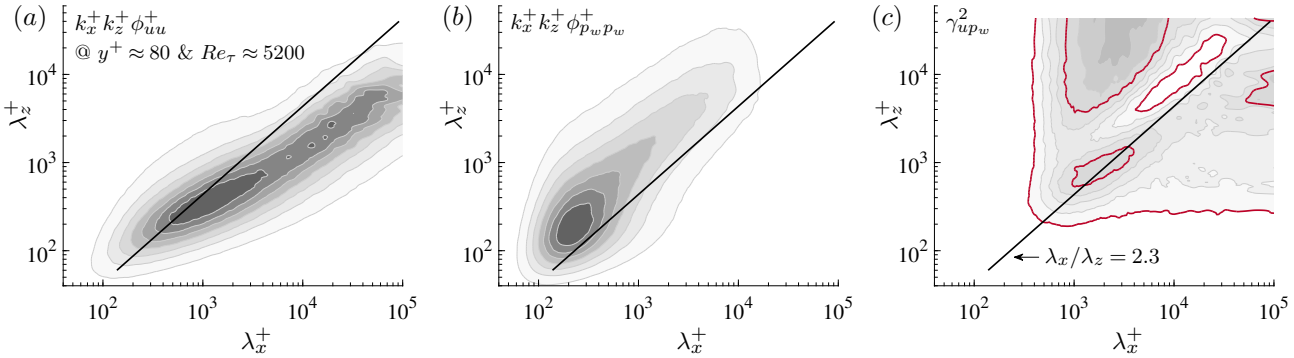

Figure 5: 2D spectrograms of (a) u and (b) p at one Re_τ and y^+, as indicated in the figure. The gray scale contour shows 7 iso-contours ranging up to the maximum value. (c) 2D linear coherence of u and p_w, for the same Re_τ and y^+ as (a,b); the solid, coloured iso-contours correspond to two contour values of $\gamma^2_{up_w} = [0.05;\ 0.25]$.

shown by the $\lambda_x/y \approx 8.5$ on fig. 1b). The v fluctuations also consistently lean forward with the same angle as was found for u, namely $\alpha \approx 30°$.

Observations made on the basis of figs. 2 and 3 are summarized in fig. 4. When coherent motions are thought of as hairpins (and packets of them), the spanwise centre is associated with a negative streamwise fluctuation while the v-fluctuations induced by the vortical motions of the packet reside at a shorter streamwise wavelength. This is reflective of the ridges of peak-coherence for u and v at $\lambda_x/y \approx 14$ and 8.5, respectively. Mechanistically, v fluctuations induce wall-pressure through a pressure stagnation when directed towards the wall, while u fluctuations are anti-correlated to pressure fluctuations because of the balance/exchange of pressure and momentum.

2D analysis in the streamwise–spanwise plane

A 1D spectral analysis along x lumps all spanwise information together. In order to inspect which spanwise scales of velocity fluctuations are coherent with the the spanwise scales of wall-pressure, we move towards a 2D analysis in the streamwise–spanwise plane. At first the 2D spectrograms of streamwise velocity fluctuations, $\phi_{uu}(\lambda_x,\lambda_z)$, and pressure fluctuations, $\phi_{p_wp_w}(\lambda_x,\lambda_z)$, are shown for $y^+ = 80$ at $Re_\tau \approx 5200$ in figs. 5a and 5b. When integrated out its λ_z dependence, the 1D spectra of figs. 1a,c are obtained at $y^+ = 80$ (for u) and at the wall (for p_w). A 2D coherence is a generalization of eq. (2) and results in the following for the streamwise velocity $u(x,y_e,z)$ and wall-pressure $p_w(x,z)$ (where y_e is an evaluation location for the velocity):

$$\gamma^2_{up_w}(\lambda_x,\lambda_z) = \frac{|\phi_{up_w}(\lambda_x,\lambda_z)|^2}{\phi_{uu}(\lambda_x,\lambda_z)\,\phi_{p_wp_w}(\lambda_x,\lambda_z)}. \quad (3)$$

Note again that the y_e argument of the wall-normal location is omitted in eq. (3) for brevity. When computing the 2D coherence for the same data as for which the 2D (auto-)spectrograms were plotted in figs. 5a,b, the coherence-contour of fig. 5c is obtained. Notably, the coherence only becomes significant (when taking a threshold of $\gamma^2_{up_w} = 0.05$) for $\lambda_x^+ > 400$, agreeing to what was previously observed in fig. 2. More interesting is that the peak-coherence in 2D still resides close to $\lambda_x/y \approx 14$ (for fig. 5c equivalent to $\lambda_x^+ = 14y^+ = 1120$) and is reasonably symmetric around $\lambda_x/\lambda_z = 2.3$. The latter implies that the wall-pressure-coherent u velocity structures are roughly twice as long as they are wide.

An important note of caution for interpreting the coherence is that a high value is not always relevant in terms of absolute energies (since the coherence is energy-normalized). For instance, at $(\lambda_x^+,\lambda_z^+) = (10^3,10^4)$ in fig. 5c, the coherence is just over $\gamma^2_{up_w} = 0.25$, even though the absolute energy in the u fluctuations is extremely low (and not visible in the contour plot of fig. 5a).

In order to now assess the trend of the 2D coherence for p_w and u with height and with Re_τ, we move towards the representation in fig. 6 and start with fig. 6b, which

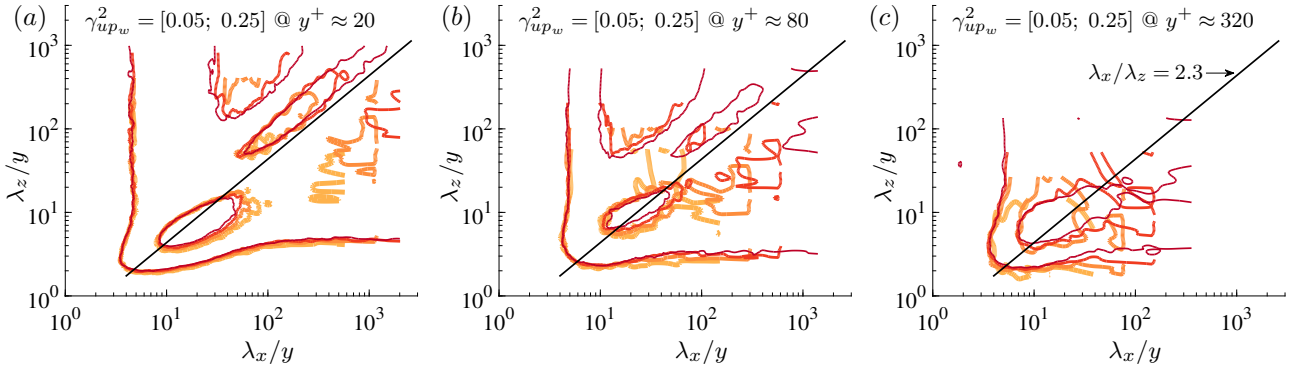

Figure 6: 2D linear coherence of u and p_w, for all Re_τ cases and for three wall-normal positions, indicated in each of the three sub-figures (a-c). Note that the wavelengths λ_x and λ_z are represented with a wall-scaling (normalized by y). The solid, coloured iso-contours correspond to the same two contour values as were considered in fig. 5c, $\gamma^2_{up_w} = [0.05;\ 0.25]$.

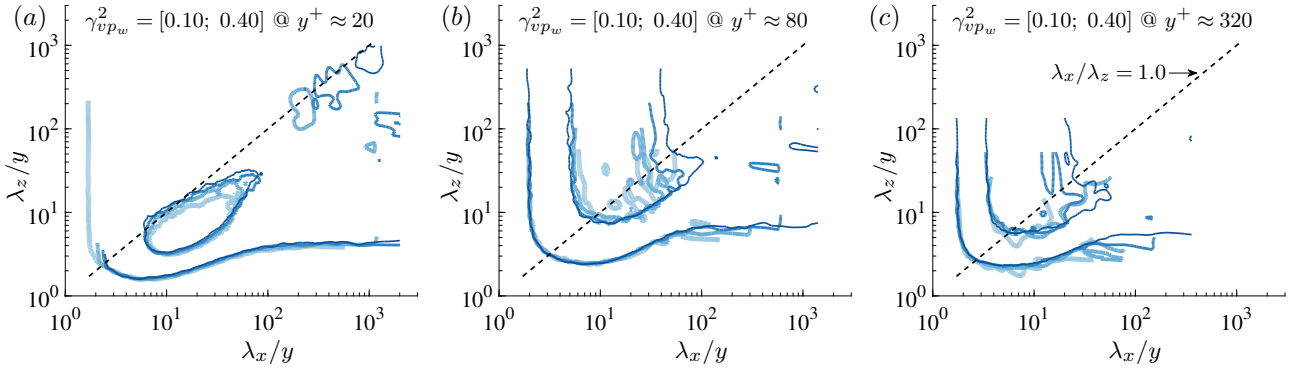

Figure 7: Similar to fig. 6 but for v and p_w, instead of u and p_w. The solid, coloured iso-contours correspond to two contour values of $\gamma^2_{vp_w} = [0.10;\ 0.40]$.

is valid for a height of $y^+ \approx 80$. For all cases of Re_τ, two sets of iso-contours of the coherence are shown; the same colour scale as in fig. 2 is adopted. For the most dark-red case ($Re_\tau \approx 5200$), the two iso-contours are similar to the ones shown in fig. 5c. Similar plots can be generated for lower y^+ locations (fig. 6a for $y^+ \approx 20$) and higher locations (fig. 6c for $y^+ \approx 320$). Since the axes in all sub-figures are scaled with the respective y location, a match of the iso-contours corresponds to a self-similar scaling in y. This is the case when comparing figs. 6a-c. Moreover, these graphs are direct evidence of a Reynolds number invariant behaviour of the coherence because all Re_τ iso-contours collapse.

Note that when the 2D coherence analysis is repeated for p_w and v (instead of u), the resultant assessment for the scaling behavior is shown in fig. 7. Since the iso-contours of $\gamma^2_{vp_w}$ collapse also, it can be concluded that the 2D coherence for p_w and u, and p_w and v, adhere to a Reynolds number-invariant wall-scaling with y. Because it was already derived in the 1D analysis that the wall-pressure-coherent v fluctuations are half the size of the corresponding u fluctuations, the same is observed in the 2D coherence. While the 2D coherence of p_w and u peaks around $\lambda_x/\lambda_z = 2.3$, the coherence of p_w and v peaks around $\lambda_x/\lambda_z = 1.0$, illustrating that the shorter streamwise extent of wall-coherent v fluctuations are roughly of the same width. That is, we can conclude that the ridge of coherence for p_w and u scales as $\lambda_x : \lambda_z : y \propto 14 : 6 : 1$, while for p_w and v this scales as $\lambda_x : \lambda_z : y \propto 8.5 : 8.5 : 1.0$ (note that a coherence analysis for turbulent pipe flow at high Reynolds numbers resulted in an aspect ratio of 7:1:1 for the velocity fluctuations with their skin-friction footprint, see Baidya *et al.*, 2019). Finally, the coherence magnitude of v is roughly a factor two higher (note the different iso-contour between figs. 6 and 7.

CONCLUDING REMARKS

This work examined the scaling behaviour of the coherence between the turbulent velocity fluctuations and the wall-pressure field. For streamwise data of u and v (in relation to the wall-pressure p_w), the strongest coupling appears at $\lambda_x/y \approx 14$ and $\lambda_x/y \approx 8.5$, respectively. The 2D extension of the analysis (as a function of λ_x and λ_z) revealed that the peak-coherence for p_w and u still resides close to $\lambda_x/y \approx 14$ and is reasonably symmetric around $\lambda_x/\lambda_z = 2.3$. The 2D coherence for p_w and v peaks around $\lambda_x/\lambda_z = 1.0$. Both the 2D coherence for p_w and u, and p_w and v, adhere to a wall-scaling with y. Statistically this can be summarized as that the ridge of coherence for p_w and u scales following $\lambda_x : \lambda_z : y \propto 14 : 6 : 1$, while for p_w and v the scaling is $\lambda_x : \lambda_z : y \propto 8.5 : 8.5 : 1.0$. An analysis of the kernel's phase demonstrated that both the coherent fluctuations of the streamwise and wall-normal velocity obey a forward-leaning inclination angle of $\alpha \approx 30°$. With the data spanning a decade in friction Reynolds num-

ber $Re_\tau \sim 550 - 5200$ and a very good Reynolds number invariant trend, the current work allows for an extrapolation of the identified scaling laws to higher Re_τ conditions. The scaling behaviours will therefore aid the efficacy efficacy of real-time controllers, by for instance the implementation of data-derived FIR filters to only control velocity structures that are captured through wall-pressure measurements.

REFERENCES

Abbassi, M. R., Baars, W. J., Hutchins, N. & Marusic, I. 2017 Skin-friction drag reduction in a high-Reynolds-number turbulent boundary layer via real-time control of large-scale structures. *Int. J. Heat Fluid Flow* **67**, 30–41.

Baars, W. J., Hutchins, N. & Marusic, I. 2016 Spectral stochastic estimation of high-Reynolds-number wall-bounded turbulence for a refined inner-outer interaction model. *Phys. Rev. Fluids* **1**, 054406.

Baars, W. J., Hutchins, N. & Marusic, I. 2017 Self-similarity of wall-attached turbulence in boundary layers. *J. Fluid Mech.* **823**, R2.

Baidya, R., Baars, W. J., Zimmerman, S., Samie, M., Hearst, R. J., Dogan, E., Mascotelli, L., Zheng, X., Bellani, G., Talamelli, A., Ganapathisubramani, B., Hutchins, N., Marusic, I., Klewicki, J. & Monty, J. P. 2019 Simultaneous skin friction and velocity measurements in high Reynolds number pipe and boundary layer flows. *J. Fluid Mech.* **871**, 377–400.

Brunton, S. L. & Noack, B. R. 2015 Closed-loop turbulence control: Progress and challenges. *Appl. Mech. Rev.* **67** (5), 050801.

del Álamo, J. C. & Jiménez, J. 2003 Spectra of the very large anisotropic scales in turbulent channels. *Phys. Fluids* **15** (6), L41–L44.

Deshpande, R., Chandran, D., Monty, J. P. & Marusic, I. 2020 Two-dimensional cross-spectrum of the streamwise velocity in turbulent boundary layers. *J. Fluid Mech.* **890**, R2.

Encinar, M. P. & Jiménez, J. 2019 Logarithmic-layer turbulence: A view from the wall. *Phys. Rev. Fluids* **4**, 114603.

Farabee, T. M. & Casarella, M. J. 1991 Spectral features of wall pressure fluctuations beneath turbulent boundary layers. *Phys. Fluids A* **3** (10), 2410–2420.

Ghaemi, S. & Scarano, F. 2013 Turbulent structure of high-amplitude pressure peaks within the turbulent boundary layer. *J. Fluid Mech.* **735**, 381–426.

Gibeau, B. & Ghaemi, S. 2021 Low- and mid-frequency wall-pressure sources in a turbulent boundary layer. *J. Fluid Mech.* **918**, A18.

Hwang, Y. F., Bonness, W. K. & Hambric, S. A. 2009 Comparison of semi-empirical models for turbulent boundary layer wall pressure spectra. *J. Sound Vibr.* **319**, 199–217.

Klewicki, J. C., Priyadarshana, P. J. A. & Metzger, M. M. 2008 Statistical structure of the fluctuating wall pressure and its in-plane gradients at high reynolds number. *J. Fluid Mech.* **609**, 195–220.

Lasagna, D., Orazi, M. & Iuso, G. 2013 Multi-time delay, multi-point linear stochastic estimation of a cavity shear layer velocity from wall-pressure measurements. *Phys. Fluids* **25**, 017101.

Lee, M. & Moser, R. D. 2015 Direct numerical simulation of turbulent channel flow up to $Re_\tau = 5200$. *J. Fluid Mech.* **774**, 395–415.

Lee, M. & Moser, R. D. 2019 Spectral analysis of the budget equation in turbulent channel flows at high Reynolds number. *J. Fluid Mech.* **860**, 886–938.

Liu, C. & Gayme, D. F. 2020 An input–output based analysis of convective velocity in turbulent channels. *J. Fluid Mech.* **888**, A32.

Mathis, R., Hutchins, N. & Marusic, I. 2009 Large-scale amplitude modulation of the small-scale structures in turbulent boundary layers. *J. Fluid Mech.* **628**, 311–337.

Naguib, A. M., Wark, C. E. & Juckenhöofel, O. 2001 Stochastic estimation and flow sources associated with surface pressure events in a turbulent boundary layer. *Phys. Fluids* **13** (9), 2611–2626.

Naka, Y., Stanislas, M., Foucaut, J.-M., Coudert, S., Laval, J.-P. & Obi, S. 2015 Space–time pressure–velocity correlations in a turbulent boundary layer. *J. Fluid Mech.* **771**, 624–675.

Panton, R. L., Lee, M. & Moser, R. D. 2017 Correlation of pressure fluctuations in turbulent wall layers. *Phys. Rev. Fluids* **2**, 094604.

Rathnasingham, R. & Breuer, K. S. 2003 Active control of turbulent boundary layers. *J. Fluid Mech.* **495**, 209–233.

Samie, M., Baars, W. J., Rouhi, A., Schlatter, P., Örlu, R., Marusic, I. & Hutchins, N. 2020 Near wall coherence in wall-bounded flows and implications for flow control. *Int. J. Heat Fluid Flow* **86**, 108683.

Thomas, A. S. W. & Bull, M. K. 1983 On the role of wall-pressure fluctuations in deterministic motions in the turbulent boundary layer. *J. Fluid Mech.* **128**, 283–322.

Tinney, C. E., Coiffet, F., Delville, J., Glauser, M. N., Jordan, P. & Hall, A. M. 2006 On spectral linear stochastic estimation. *Exp. Fluids* **41** (5), 763–775.

Van Blitterswyk, J. & Rocha, J. 2017 An experimental study of the wall-pressure fluctuations beneath low Reynolds number turbulent boundary layers. *J. Acoust. Soc. Am.* **141** (2), 1257–1268.

Willmarth, W. W. 1975 Pressure fluctuations beneath turbulent boundary layers. *Annu. Rev. Fluid Mech.* **7**, 13–36.